PHYSICS

Energy penetration into arrays of aligned nanowires irradiated with relativistic intensities: Scaling to terabar pressures

Clayton Bargsten,[1] Reed Hollinger,[1] Maria Gabriela Capeluto,[2] Vural Kaymak,[3] Alexander Pukhov,[3] Shoujun Wang,[1] Alex Rockwood,[4] Yong Wang,[1] David Keiss,[4] Riccardo Tommasini,[5] Richard London,[5] Jaebum Park,[5] Michel Busquet,[6] Marcel Klapisch,[6] Vyacheslav N. Shlyaptsev,[1] Jorge J. Rocca[1,4]*

Ultrahigh-energy density (UHED) matter, characterized by energy densities >1 × 10^8 J cm^{-3} and pressures greater than a gigabar, is encountered in the center of stars and inertial confinement fusion capsules driven by the world's largest lasers. Similar conditions can be obtained with compact, ultrahigh contrast, femtosecond lasers focused to relativistic intensities onto targets composed of aligned nanowire arrays. We report the measurement of the key physical process in determining the energy density deposited in high-aspect-ratio nanowire array plasmas: the energy penetration. By monitoring the x-ray emission from buried Co tracer segments in Ni nanowire arrays irradiated at an intensity of 4 × 10^{19} W cm^{-2}, we demonstrate energy penetration depths of several micrometers, leading to UHED plasmas of that size. Relativistic three-dimensional particle-in-cell simulations, validated by these measurements, predict that irradiation of nanostructures at intensities of >1 × 10^{22} W cm^{-2} will lead to a virtually unexplored extreme UHED plasma regime characterized by energy densities in excess of 8 × 10^{10} J cm^{-3}, equivalent to a pressure of 0.35 Tbar.

INTRODUCTION

Laboratory creation of matter in the ultrahigh-energy density (UHED) regime is of great interest for the realization of inertial confinement fusion (*1*, *2*), to further the understanding of atomic processes in astrophysical and extreme laboratory environments (*3*–*5*), and to generate intense sources of x-rays and high-energy particles (*6*, *7*). However, the creation of matter in this regime in the laboratory has been limited to the central hot spot of the spherically imploded capsule in inertial confinement fusion experiments conducted using the world's highest-energy lasers (*8*, *9*). The ability to create UHED matter using smaller facilities is thus of great interest to make this extreme plasma regime more accessible for fundamental studies and applications. One such application is the efficient conversion of optical laser light into bright flashes of x-rays, which requires the radiative lifetime of the plasma to be shorter than the hydrodynamic cooling time. This, in turn, demands simultaneously having a large collision rate (and therefore a large density of energetic electrons) and a large plasma size. However, heating a large UHED plasma volume is a challenge that even many of today's most powerful lasers fall short of achieving when irradiating solid slab targets. In this conventional heating scheme, the leading edge of the laser pulse rapidly creates a plasma blow-off, which prevents the remainder of the laser pulse from directly heating the solid region of the target. Heating by hot electrons using today's most energetic short pulse lasers has just surpassed the boundary into the UHED regime (for example, achieving 2 Gbar). For example, temperatures of 0.6 keV at a density of 1.5 g/cc were recently reported for a 0.15-μm-thick Al foil tamped by 10 μm of plastic on both sides, irradiated by 100-J pulses of 0.5-ps duration (*10*). Simulations indicate a pressure of 0.5 Gbar, and an energy density approaching 1 × 10^8 J cm^{-3} was obtained. Similar temperatures were achieved at a density of 9 g/cc, and therefore higher pressure and energy density, using diamond tamped Al targets compressed with a pair of 200-J, long laser pulses before the arrival of the short heating pulse (*10*). Several other experiments in which pulses of 0.35- to 2-ps duration irradiated plastic foils with buried metal layers reported similar temperatures (*11*–*14*). Heating with 400-J pulses of 0.8-ps duration achieved a 5-keV surface temperature decreasing to 0.6 keV at 1.3-μm depth (*15*).

Alternatively, irradiation of high-aspect-ratio vertically aligned nanowire arrays with ultrahigh-contrast femtosecond laser pulses of only joule-level energy provides a unique combination of nearly complete optical absorption and drastically enhanced light penetration into near-solid density targets, allowing the material to be volumetrically heated deep into the UHED regime. Other types of structured targets have also been successfully used to increase absorption, as evidenced by enhanced x-ray emission from "smoked" targets (*16*), nanospheres (*17*), gratings (*18*, *19*), and "velvet" nanowire targets (*20*–*23*). However, high-aspect-ratio vertically aligned nanostructures with vacant spaces surrounding them are unique in allowing for the deep penetration of ultrafast optical laser pulse energy into the material, where light is trapped and practically totally absorbed (*24*). Electrons ripped off the nanowire surface by the large laser field are accelerated to acquire high energy in the voids. Collisions of these energetic electrons with the nanowires rapidly heat the material to extreme temperatures, causing the nanostructures to explode and rapidly fill the voids. When the gaps are filled with plasma, a continuous critical electron density layer that forbids further coupling of laser energy into the material is formed. The use of sufficiently short laser pulses allows for very efficient coupling of the pulse energy deep into the nanowire array, heating a large volume of near-solid-density material several micrometers in depth to multi–kilo–electron volt temperatures. This new approach to volumetric heating opens access to the UHED plasma regime using tabletop, joule-class, femtosecond lasers.

[1]Electrical and Computer Engineering Department, Colorado State University, Fort Collins, CO 80523, USA. [2]Departamento de Física, Universidad de Buenos Aires, Buenos Aires, Argentina. [3]Institut für Theoretische Physik, Heinrich-Heine-Universität Düsseldorf, 40225 Düsseldorf, Germany. [4]Physics Department, Colorado State University, Fort Collins, CO 80523, USA. [5]Lawrence Livermore National Laboratory, Livermore, CA 94551, USA. [6]ARTEP Inc., Ellicott City, MD 21042, USA.
*Corresponding author. Email: jorge.rocca@colostate.edu

Considering that the aligned nanowire arrays are highly optically absorbent, the heat penetration depth into the arrays is the key unknown parameter for determining the plasma volume heated and, thus, the deposited energy density. Here, we report the first definitive measurement of the volume of heated material in arrays of high-aspect-ratio aligned nanowires irradiated by femtosecond pulses of relativistic intensity. We present the results of experiments at an intensity of 4×10^{19} W cm^{-2} that show heating of near-solid-density matter to multi–kilo–electron volt temperatures over depths of several micrometers. The results serve to validate a model of the relativistic interaction that is used to study the physics of these unique plasmas and to predict the UHED conditions that will be achieved when the intensity is increased to the limit of currently available laser systems and beyond. As shown below, this approach promises to achieve unprecedented energy densities in excess of 8×10^{10} J cm^{-3}, equivalent to 0.35-Tbar pressures using existing ultrafast laser facilities.

The measurement technique consists of monitoring the He-α line emission from buried nanowire segments of a selected tracer material. This required growing arrays of ordered nanowires that have a compositional change along the length of each nanowire (Fig. 1, A and B). We found it advantageous to choose neighboring elements on the periodic table that have similar ionization dynamics for the top and buried (tracer) segments to form an array that does not differ significantly from one of uniform composition. This selection also allows the characteristic spectral lines of both materials, such as the He-α lines, to be recorded simultaneously within the spectral window of a single crystal spectrometer. In this experiment, the composition of the top segment of the nanowires was nickel (Z = 28), and the buried tracer element was cobalt (Z = 27). The experiments were simulated using the combination of a relativistic three-dimensional (3D) particle-in-cell (PIC) code in combination with a transient atomic kinetics and radiation transport model.

RESULTS AND DISCUSSION

The experiments were conducted by irradiating the segmented nanowire arrays with λ = 400 nm, ultrahigh-intensity contrast (>10^{12}) pulses of 0.6 J of energy, and 55-fs full width at half maximum (FWHM) duration from a frequency-doubled titanium-sapphire laser at Colorado State University (see Materials and Methods). The ultrahigh contrast is crucial to preserve the nanowires until the arrival of the intense laser pulse. The laser pulses were focused onto the nanowire arrays using an f/2.7 parabolic mirror. The emitted x-ray radiation was analyzed using a von Hamos crystal spectrometer (*25*) in which a mica crystal spectrally disperses the signal onto a 2D back-thinned charge-coupled device (CCD) sensor array.

Figure 1C shows a single-shot spectrum from an irradiated dual composition Ni-Co nanowire array in which the He-like lines of the Ni and Co segments were simultaneously recorded. Both materials have a high Young's modulus, which facilitates the growth of arrays of well-aligned, high-aspect-ratio nanowires. The nanowire arrays were grown by sequential electrodeposition of the selected metals into porous anodic aluminum oxide membranes. Subsequent dissolution of the membranes results in freestanding aligned nanowire arrays (see Materials and Methods). The compositional change was thus created by first growing 3- to 4-μm-long Co nanowires at the base of each array followed by the growth of segments of Ni of several selected lengths on top. The change in composition along the nanowires is visible in the scanning electron microscope energy-dispersive spectroscopy (EDS) measurement shown in Fig. 1B. The arrays used in the experiment consisted of 55-nm- diameter nanowires spaced such that the array had an average atomic density corresponding to 13% of solid density.

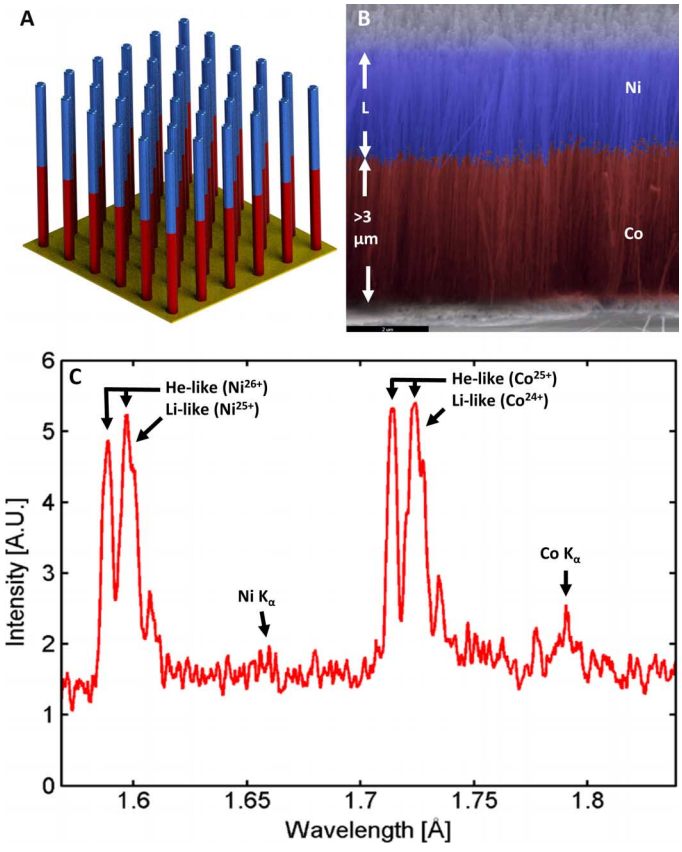

Fig. 1. Schematic diagram, composition map, and x-ray spectrum of a two-composition Ni-Co nanowire array. (**A**) Schematic diagram of segmented two-composition Ni-Co nanowire array. The top Ni segment ranges in length from 1 to 6 μm. The nanowires are 55 nm in diameter and form an array that is 13% of solid density. (**B**) Scanning electron microscopy image with energy-dispersive spectroscopic elemental composition measurement indicating the concentration of Ni (blue) and Co (red). (**C**) Example spectra showing the He-like line dominance over the K_α lines for the two elements as recorded using a von Hamos crystal spectrometer. A.U., arbitrary units.

Figure 2 shows a series of measured spectra resulting from irradiating Ni-Co nanowire targets in which the top wire segment of Ni increases in length from 1.5 to 5 μm. The spectra show an increase in the He-like Ni line emission signal and a corresponding decrease in the He-like Co signal as the length of the top Ni nanowire segment increases. In the case of the array with a 1.5-μm-long top Ni layer, the Co lines dominate. This is a first clear indication that the heat penetrates more than 3 μm along the length of the nanowires. A decrease in intensity of the Co lines is subsequently seen as the length of the top nickel layer is increased. The emission from He-like Co ions is observed for targets with up to 4 μm of Ni on top. As the top nickel layer reaches 5 μm in thickness, the Co lines decrease in intensity to a level near that of the continuum background signal that results from bremsstrahlung and radiative recombination. In agreement with the simulations discussed below, this demonstrates that sufficient heat to ionize Co ions to the He-like stage penetrates at least 4-μm-deep into the near-solid-density material. Figure 3 plots the measured peak intensity of the Co and Ni He-α lines as a function of Ni nanowire segment length. The Ni lines become stronger as the

length of the top segment of this material is increased up to 3 to 4 μm, the length beyond which their strength saturates. Simultaneously, the strength of the Co lines decreases until they disappear into the continuum when the Ni segments reach 5 μm in length.

Simulations of the x-ray emission spectra of arrays with top Ni segments of different length were conducted with a transient atomic kinetics and radiation transport model that uses the electron energy distribution computed by the relativistic 3D PIC simulations (see Materials and Methods). The synthetic spectra (Fig. 4, top) closely replicate the observed features of the experimental data. The bottom panel of Fig. 4 illustrates the agreement between the measured and simulated Co/Ni line ratios as a function of Ni wire segment length. Figure 5 shows the simulated spatial distribution of He-like Ni and Co ions for an array with a top segment of 3-μm Ni nanowires after the peak of the laser pulse. It illustrates the generation of He-like Co ions several micrometers under the top Ni nanowire layer. The agreement between measurement and simulations validates the model, which is used below to predict the plasma conditions that could be obtained by increasing the irradiation intensity.

The energy density and pressure for hot electron gases are given by integrals of the energy and momentum-velocity product, weighted by the distribution function. We have calculated the energy density directly from the particle data from the PIC simulation and estimated the pressure from that, using a formula for an equilibrium relativistic gas, accurate to 1% (see Materials and Methods) (*26*). Computed maps of the kinetic energy density at four different times during the plasma evolution are shown in Fig. 6. Optical-field ionization (OFI) is observed to begin the heating process at the nanowire surface, with the strong electric field of the laser pulse stripping electrons and creating ionization states up to $Z = 18$. The electrons are rapidly accelerated into the gaps. Collisional electron impact ionization produces higher ionization states as the hot electron population deposits its energy deep into the nanowire cores. The electrons stripped from the wires are accelerated toward the substrate. Charge balance demands the generation of a large laser-induced return current through the nanowires. The resulting strong quasi-static self-generated azimuthal magnetic field pinches the

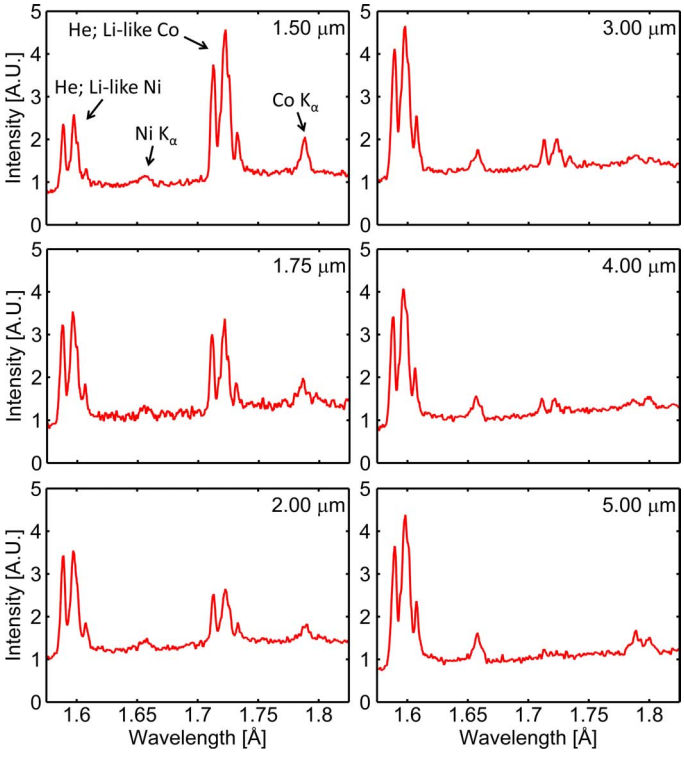

Fig. 2. Measured spectra of Ni-Co–segmented nanowire arrays with different lengths of Ni wires (listed in the top right corner of each plot) on top of cobalt wires, irradiated by 55-fs pulses at an intensity of ~4 × 10^{19} W cm^{-2}. The vertically aligned wires are 55 nm in diameter and form an array that has an average atomic density that is 13% of solid density. Lines of He-like and Li-like Ni and Co are visible along with their respective K_α lines.

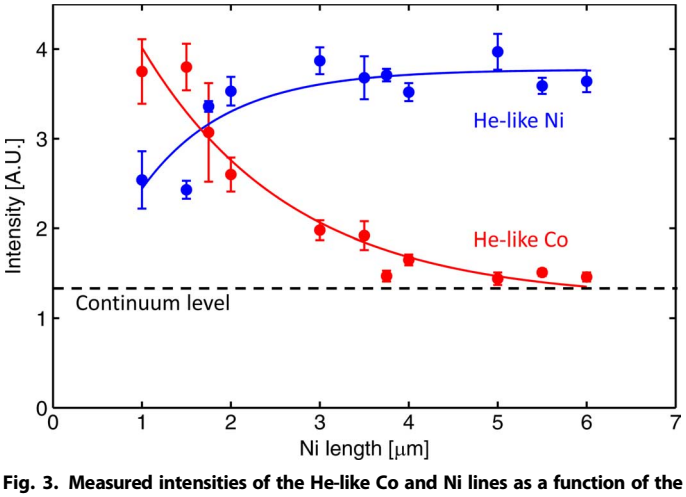

Fig. 3. Measured intensities of the He-like Co and Ni lines as a function of the length of the top Ni nanowire segment. The target and laser parameters are the same as those in Fig. 2.

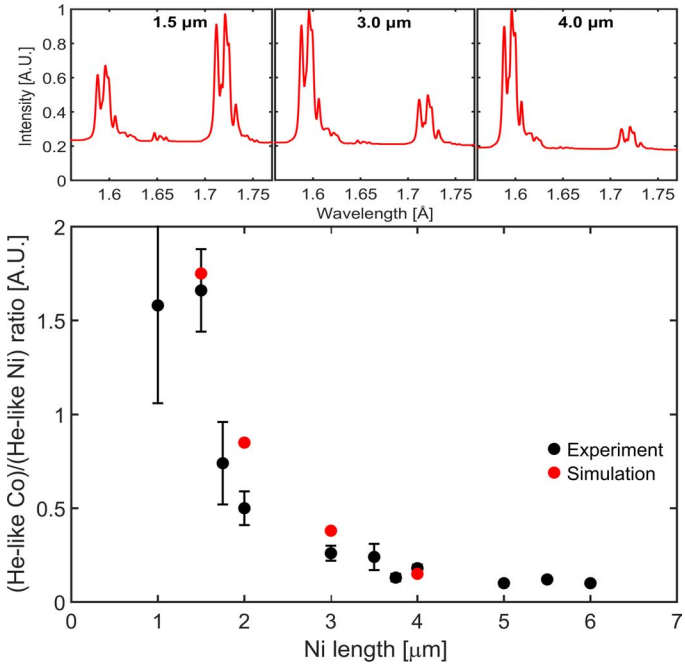

Fig. 4. Simulated spectra corresponding to arrays with different wire lengths used in the experiment are shown in the top three plots. The target and laser parameters are the same as those in Fig. 2. Measured and simulated (Co He-α)/(Ni He-α) line ratios as a function of Ni nanowire segment length are shown on the bottom.

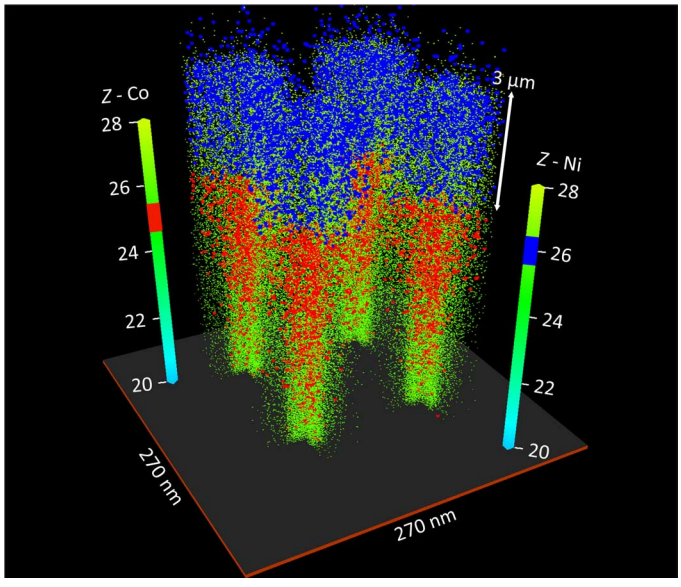

Fig. 5. PIC simulation of the density of He-like ions in an array composed of segments of vertically aligned Ni and Co nanowires (blue, He-like Ni; red, He-like Co). The target and laser parameters are the same as those in Fig. 2. The top Ni wires are 3.0 μm in length. The laser pulse impinges from the top at normal incidence to the array.

nanowires into a hot, extremely dense plasma (*27*). A plasma density surpassing 10^{24} cm^{-3} with an energy density of 22 GJ cm^{-3} and pressure of 125 Gbar is quickly reached within the wires near their tips (+4-fs frame; Fig. 6). The laser pulse continues to propagate down the length of the wires and deep into the array as long as the interwire gaps remain free of dense plasma. As the wires expand, the interwire gaps are filled with a supercritical-density plasma. Collisions homogenize the plasma, creating a uniform plasma layer several micrometers thick in which the atoms are ionized up to the He-like stage observed in the measurements. In the two earliest frames in Fig. 6 (+4 and +44 fs), the wire tips appear to be loosely connected by regions of higher energy density. This is a result of the array geometry in which the gaps are narrower in the directions directly between wires. These narrower gap regions thus fill with particles more quickly and reach higher-energy densities faster than the diagonal regions. Expansion of the wires continues to progressively close the interwire gaps along the length of the wires (+124-fs frame; Fig. 6) until the whole target cross section is filled with material at an energy density of 1 GJ cm^{-3} and pressure of 7 Gbar (+304-fs frame; Fig. 6). A thermalized electron temperature of ~14 keV is reached over the plasma volume with an average electron density greater than 3×10^{23} cm^{-3}. Even higher plasma densities can be obtained by irradiating arrays with higher wire filling factors, arrays made of a higher Z material, or a combination of both. As an example in the Supplementary Materials, we include a spectrum of a Ni nanowire target with an average atomic density corresponding to 30% of solid density irradiated at an intensity of 4×10^{19} W cm^{-2} (fig. S1). The spectrum is again dominated by He-like (Ni^{+26}) and Li-like (Ni^{+25}) lines, which indicate the high degree of ionization is maintained. In this case, the average electron

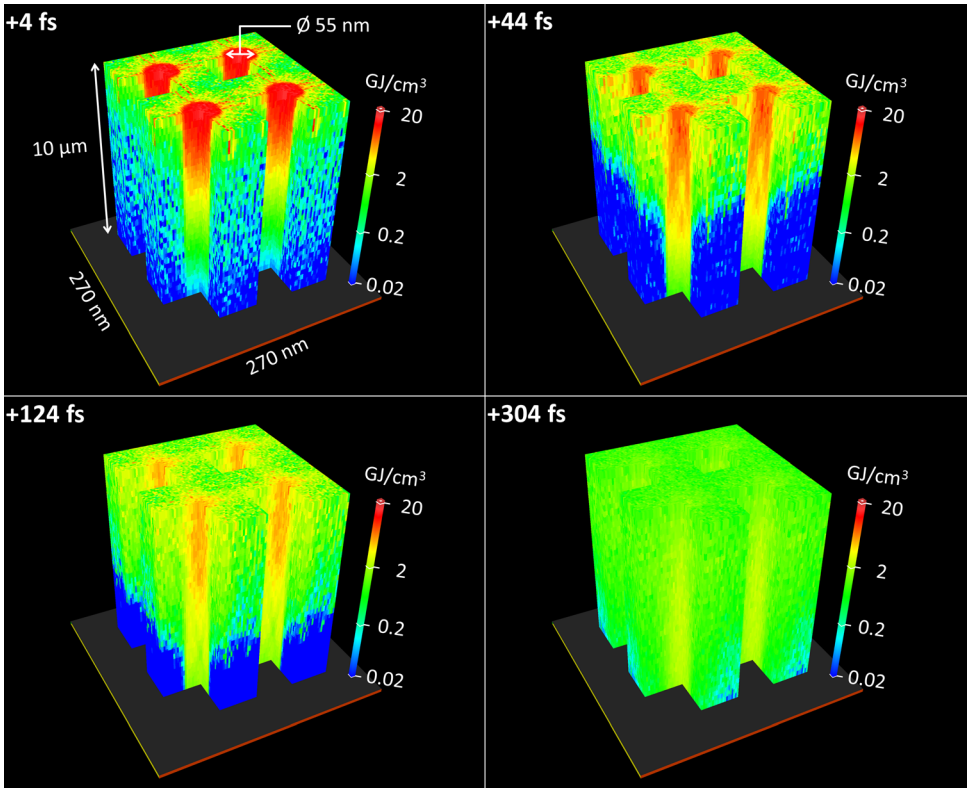

Fig. 6. ED distribution computed by PIC simulation. The target and laser parameters are the same as those in Fig. 5. Each frame corresponds to a different time with respect to the peak of the laser pulse as indicated by the time stamp in the top left corner of each frame. The laser pulse impinges into the array from the top at normal incidence.

density of the homogenized plasma increases up to ~7 × 10^{23} cm^{-3}, nearly 100 times the critical density.

We conducted additional PIC simulations to predict the plasma conditions that could be achieved by further increasing the laser irradiation intensity to 1 × 10^{22} W cm^{-2} (a_0 = 34). The results suggest the generation of unprecedented energy densities and pressures. This is illustrated in Fig. 7 for an array of 400-nm-diameter Au nanowires with an average atomic density corresponding to 12% of solid density, irradiated with a 30-fs duration pulse. The plasma density in the gold nanowires during the nanoscale pinch compression phase reaches 2 × 10^{25} cm^{-3}, which corresponds to nearly 3200 times the critical density (fig. S2). Other laser-target configurations could reach even higher densities during the nanopinch (for example, 6 × 10^{25} cm^{-3}). These extreme peak densities would approach those obtained from fusion hot spots using megajoule laser energies at the National Ignition Facility (~1 × 10^{26} cm^{-3}) (*28*) while potentially reaching higher temperatures. The energy density within the nanowires is predicted to reach a peak value of 2 TJ cm^{-3}, equivalent to a pressure of 7 Tbar near the end of the laser pulse (+21-fs frame; Fig. 7). The expansion of the heated nanowires is computed to create a plasma layer in which the energy density is 80 GJ cm^{-3}, equivalent to a 0.35-Tbar pressure (+500-fs frame; Fig. 7), larger than the solar interior pressure. The electron energy can be described by a two-temperature distribution, which rapidly thermalizes into a single-temperature distribution defined by an electron temperature of ~500 keV, 500 fs after the peak of the laser pulse (see fig. S3).

Figure 8 shows that the gold atoms are predicted to reach extreme degrees of ionization. At 20 fs after the peak of the laser pulse, Ni-like Au ions are dominant, whereas ions up to Ne-like (Au^{+69}) are also predicted to be present within the nanowires for depths up to several micrometers. A few hundred femtoseconds after the end of the laser pulse (for example, +500 fs in Fig. 7), the plasma is still hot, and ionization still continues, creating charge states up to Au^{+70}. Moreover, irradiation of an array of 150-nm-diameter Au nanowires with an initial average density of 30% solid is predicted to result in denser plasma in which Au atoms near the tip of the array could potentially be ionized to the Be-like stage (Au^{+75}). Irradiation of higher Z elements is expected to result in even higher charge states.

These extreme energy densities offer important advantages for the efficient generation of ultrashort pulses of x-rays and neutrons. In the case of x-ray generation, the large plasma density decreases the radiative lifetime. This results in an increase in the hydrodynamic-to-radiative lifetime ratio that leads to a large increase in conversion efficiency. Accordingly, in experiments we have conducted with aligned gold nanowires, we have measured a record conversion efficiency into ultrashort pulses of >1-keV photons of 10% in 2π str. In the case of the generation of neutrons by deuterium-deuterium or deuterium-tritium fusion reactions, the high density of energetic ions is an important advantage because the reaction rate is proportional to the square of the density. These aligned nanostructure plasmas share some similarities to the efficient volumetric heating of clusters in a supersonic gas

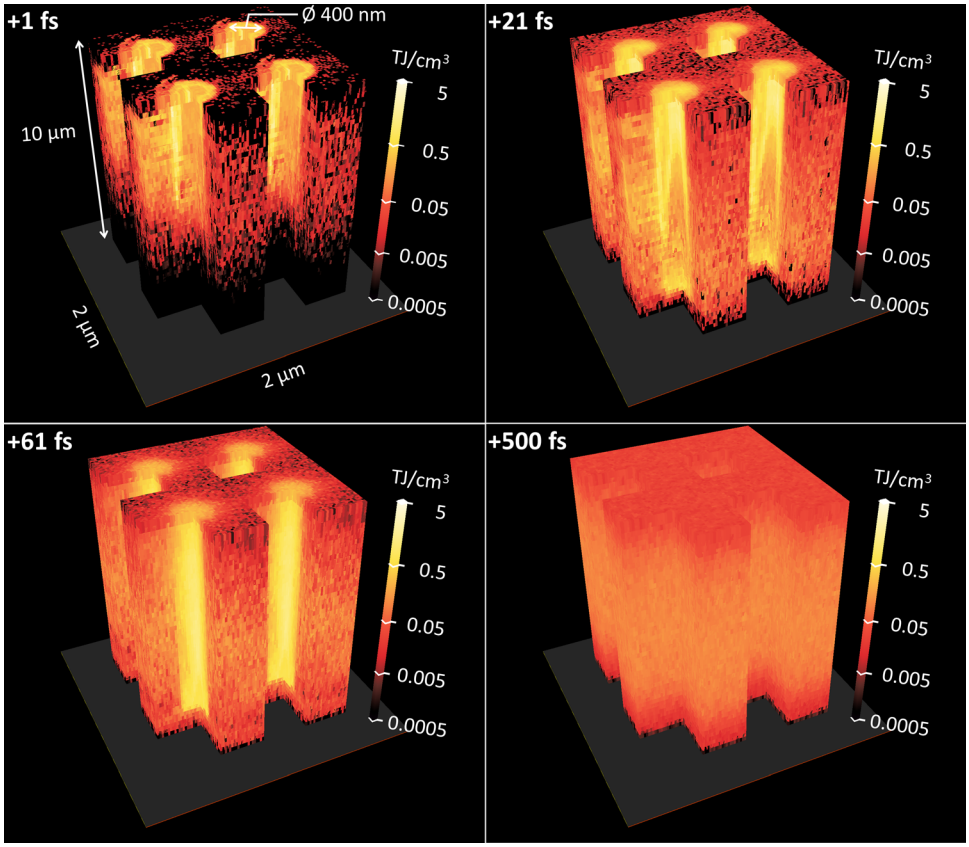

Fig. 7. PIC-simulated energy density distribution in an array of vertically aligned 400-nm-diameter Au nanowires irradiated with an intensity of 1 × 10^{22} W cm^{-2} (a_0 = 34) using a 400-nm wavelength pulse of 30-fs duration. The average atomic density is 12% of solid density. Each frame corresponds to a different time with respect to the peak of the laser pulse. The laser pulse impinges into the array from the top at normal incidence.

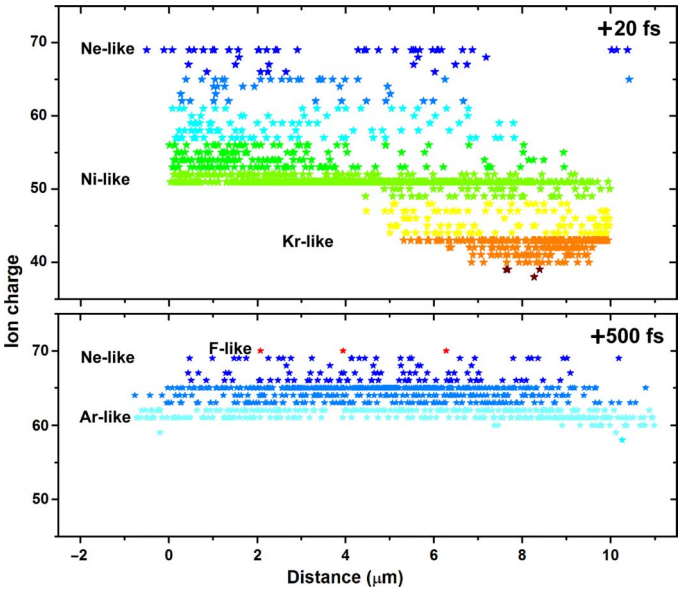

Fig. 8. Ion charge distribution as a function of depth for an array of 400-nm-diameter Au nanowires with 12% of solid density, irradiated at an intensity of 1 × 10^{22} W cm^{-2} as in Fig. 7. This plot was obtained by randomly choosing a fraction of the ions and placing a star at each charge and position. Groups of ionization stages are assigned different colors (for example, $Z = 66$ to 70 is blue) to accentuate the ion distribution and identify rare ions, such as the F-like ions in the bottom.

jet (*29*), but with the additional advantage of having several orders of magnitude higher-average density, potentially leading to record fusion neutron yields with compact lasers.

It is also of interest to gain insight into how the energy density scales with irradiation intensity. However, this scaling would have a very limited range of applicability without the simultaneous change of the nanostructure target parameters, for example, the nanowire diameter. The ideal configuration for many applications, such as neutron generation, efficient conversion into x-rays, and creation of highest-Z ions, requires obtaining a plasma lifetime as large as possible compared to the characteristic times of the fusion reactions, radiation cooling, and ionization time, respectively. That means that the laser energy deposition depth has to be typically of the order of the laser focal spot size, which, in our case, is 4 to 6 μm. As the irradiation intensity is increased, scaling of the interwire distance is required to maintain this constant energy penetration depth. Otherwise, not only would the laser energy penetration depth be either too short or too long, but the efficiency of the laser energy deposition would also decrease. This is because there exists a time for the closure of the interwire space for the laser by the expanding plasma, after which a continuous critical density layer is formed, which increases the fraction of laser energy reflected (*24*). Therefore, to determine the energy density scaling, we used the strategy of keeping the energy penetration depth approximately constant and comparable to focal spot size while scaling the interwire spacing and nanowire diameter (the latter is required to keep the average atomic density constant). For this case of approximately constant energy deposition depth, the peak value of the energy density occurring near the end of the laser pulse is computed to scale approximately linear with intensity I, energy density α I (see fig. S4). In comparison, at later times when the nanowires are completely dissolved into a homogeneous plasma, the energy density behaves as a sublinear function of the laser intensity, energy density α $I^{0.5}$, because of the faster thermal spread of the hotter plasma at larger intensities.

In conclusion, these results open a path to obtaining unprecedented pressures in the laboratory with compact lasers for the study of high energy density physics, high ionization states of high-Z atoms in high-density plasmas, and effects of opacities at ultrahigh pressures, temperatures, and densities. The experimentally validated numerical model predicts that experiments at an increased intensity of 1 × 10^{22} W cm^{-2} will result in the generation of unprecedented Tbar-level pressures in laboratory plasmas, surpassing even those in spherical compression laser fusion experiments. These plasmas can lead to record conversion efficiency of optical laser light into ultrafast x-ray flashes and to the efficient production of ultrafast neutron pulses by fusion in near-solid-density plasmas.

MATERIALS AND METHODS

Experimental setup

The dual-composition segmented nanowire array targets were irradiated with 400-nm wavelength, 0.6-J energy laser pulses of 55-fs FWHM duration from an ultrahigh-contrast frequency-doubled titanium-sapphire laser. The ultrahigh contrast, which is necessary to prevent destruction of the nanowires before the arrival of the main pulse, was achieved by frequency doubling with an 800-μm-thick type 1 potassium dihydrogen phosphate crystal. The 400-nm second harmonic light was separated from the 800-nm fundamental beam using a series of four highly selective dichroic mirrors. These high-contrast pulses were focused to an ~5-μm-diameter spot using a 90° off-axis parabolic mirror to achieve intensities of (4 ± 1) × 10^{19} W cm^{-2} on target. The focal spot size was determined by imaging with a 10× objective onto a 12-bit CCD camera. The laser pulse duration was measured using a single-shot frequency-resolved optical gating. The laser prepulse contrast in the picosecond range was monitored with a third-order scanning autocorrelator, and in the nanosecond range, it was determined using a photodiode and a set of calibrated neutral density filters. The prepulse intensity contrast of the frequency-doubled pulse was inferred to be greater than 1 × 10^{12}. The laser pulse energy was monitored on a shot-by-shot basis by measuring the reflection from a 500-μm-thick, 1% reflecting, multilayer-coated beam splitter placed before the off-axis parabola.

The emitted x-ray spectrum was measured using a von Hamos crystal spectrometer (*25*). The spectrometer used the third-order reflection from a cylindrically bent mica crystal to spectrally disperse the x-ray signal onto a back-thinned 2D CCD sensor. The sensor was shielded from electromagnetic noise and visible light by an electrically and optically sealed Faraday cage, in which the diffracted x-ray signal reaches the CCD through a 12.5-μm-thick Al foil filter. The thickness of the Al foil filter was selected to also stop lower-order reflections from the mica crystal.

Vertically aligned nanowire arrays

The nanowire arrays were grown by the electrodeposition of metallic ions into porous alumina templates. The density of pores determined the average density of the nanowire array. A Watts bath (*30*) solution was used for the deposition of both nickel and cobalt materials. This galvanostatic electrodeposition allowed for the wires to be grown to a desired length inside the template pores. As the buried tracer experiments required the wires to consist of segments of two different materials, Co was first deposited in the pores to a length of 3 to 4 μm,

followed by subsequent deposition of Ni at variable lengths between 1 and 6 μm. High-resolution transmission electron microscope dispersive x-ray spectroscopy (EDS analysis) revealed that the junction region between the Co and Ni layers was smaller than 100 nm in length. Once the deposition was complete, wires were freed from the template through a dissolving process in 4 M NaOH. EDS from a scanning electron microscope was used to measure the elemental composition of the array along the length of the nanowires in each array (Fig. 1B).

Simulation tools

The relativistic 3D Virtual Laser Plasma Laboratory code (*31*) was used for the PIC simulations. The capabilities of its standard algorithms were extended by adding packages for OFI and binary collisions, including electron impact ionization. OFI was treated as an under-barrier tunneling phenomenon in the static electric field (*32*, *33*), with only sequential field ionization considered. The probabilities for Coulomb collisions between all particles in one mesh cell were calculated by a binary collision package. PIC simulations used a 3D geometry and self-consistently included ionization physics for both the Ni and Co atomic species present in the dual-composition target and for Au. A linearly polarized plane wave with 400-nm wavelength and Gaussian time envelope $a(t) = a_0 \exp(-t^2/\tau^2)$ was used to simulate the laser pulse where the normalized vector potential $a_0 = eA/mc^2 = 2.16$ corresponds to a laser intensity of $I_0 = 4 \times 10^{19}$ W cm^{-2} and a 55-fs FWHM pulse duration. The laser pulse was assumed to impinge on the nanowire array at normal incidence. The PIC simulation space consisted of a cell volume encompassing the wires and interwire gaps, as well as a space above the array to allow for expansion of the wire material as it exploded and thermalized. The simulation described all phases of the laser interaction with the nanowire array and subsequent explosion and thermalization. The code accounted for local field enhancements, field fluctuations, and resonance heating. However, bulk resonances were not considered to be present because of the average density that was higher than the critical density and the spacing of the nanowires that was smaller than the wavelength of the laser.

Simulations were also conducted with two postprocessor atomic models based on the code Radex (*34*) using atomic data from the HULLAC code (*35*). The first of these atomic models was used to compute the intensity ratio of Co/Ni He-like lines. It used the exact particle energy distribution computed with the PIC code. The second model, used to simulate the spectra (Fig. 4, top), was a very detailed atomic code that considered a large number of excited levels from all the ionization stages present. This greatly more computational intensive model used a two-temperature approximation to the electron energy distribution computed by the PIC code. Lines were computed taking into account the natural, Doppler, collisional, and Stark broadening. The Biberman-Holstein approximation (*36*, *37*) was used for radiation transport of the He-α lines. For comparison with experiments, instrumental broadening was added to the synthesized spectra (Fig. 4). The continuum was simulated by simple approximations for bremsstrahlung and radiative recombination radiation.

Estimation of the pressure from the energy density

The relationship between energy density and pressure could be readily calculated in the equilibrium case, where the distribution function was a relativistic Maxwellian, and in the nonequilibrium ultrarelativistic case, where the particle velocities were all near the speed of light. The result for an equilibrium relativistic gas is given by Synge (*38*). We used a simple approximation, accurate to 1%, given by Ryu *et al.* (*26*).

Defining β as the ratio of kinetic energy density to rest mass energy density, we found the following formula for α, the ratio of kinetic energy density to pressure

$$\alpha = \frac{6}{1 - \delta + \sqrt{\delta^2 + 6\delta + 1}} \; ; \; \delta \equiv \frac{1}{\beta}$$

The large and small β limits provide the well-known results, α = 3/2 and α = 3, respectively. The full dependence of α(β) is shown in fig. S5.

SUPPLEMENTARY MATERIALS

Supplementary material for this article is available at http://advances.sciencemag.org/cgi/content/full/3/1/e1601558/DC1

Supplementary section

fig. S1. Spectrum of an array of 55-nm-diameter Ni nanowires with an average atomic density corresponding to 30% of solid density irradiated at 4×10^{19} W cm^{-2} with an ultrahigh contrast λ = 400-nm laser pulse of 55-fs duration.

fig. S2. Computed electron density distribution in 400-nm-diameter gold nanowire irradiated at an intensity of 1×10^{22} W cm^{-2} with a 30-fs laser pulse, corresponding to the conditions in Fig. 7.

fig. S3. Electron energy distribution under the same irradiation conditions as in fig. S2 at different times with respect to the peak of the laser pulse averaged in space.

fig. S4. Computed scaling of the energy density deposited into Au nanowire arrays as a function of the irradiation intensity for two different times during the plasma evolution.

fig. S5. Ratio of kinetic energy density to pressure (α) as a function of the ratio of kinetic energy density to rest mass energy density (β).

table S1. Pressures calculated from the kinetic energy density computed by the PIC simulations using the approximation by Ryu *et al.* (*26*).

REFERENCES AND NOTES

1. S. H. Glenzer, B. J. MacGowan, P. Michel, N. B. Meezan, L. J. Suter, S. N. Dixit, J. L. Kline, G. A. Kyrala, D. K. Bradley, D. A. Callahan, E. L. Dewald, L. Divol, E. Dzenitis, M. J. Edwards, A. V. Hamza, C. A. Haynam, D. E. Hinkel, D. H. Kalantar, J. D. Kilkenny, O. L. Landen, J. D. Lindl, S. LePape, J. D. Moody, A. Nikroo, T. Parham, M. B. Schneider, R. P. J. Town, P. Wegner, K. Widmann, P. Whitman, B. K. F. Young, B. Van Wonterghem, L. J. Atherton, E. I. Moses, Symmetric inertial confinement fusion implosions at ultra-high laser energies. *Science* **327**, 1228–1231 (2010).
2. O. A. Hurricane, D. A. Callahan, D. T. Casey, P. M. Celliers, C. Cerjan, E. L. Dewald, T. R. Dittrich, T. Döppner, D. E. Hinkel, L. F. Berzak Hopkins, J. L. Kline, S. Le Pape, T. Ma, A. G. MacPhee, J. L. Milovich, A. Pak, H.-S. Park, P. K. Patel, B. A. Remington, J. D. Salmonson, P. T. Springer, R. Tommasini, Fuel gain exceeding unity in an inertially confined fusion implosion. *Nature* **506**, 343–348 (2014).
3. B. A. Remington, R. E. Rudd, J. S. Wark, From microjoules to megajoules and kilobars to gigabars: Probing matter at extreme states of deformation. *Phys. Plasmas* **22**, 090501 (2015).
4. S. Fujioka, H. Takabe, N. Yamamoto, D. Salzmann, F. Wang, H. Nishimura, Y. Li, Q. Dong, S. Wang, Y. Zhang, Y.-J. Rhee, Y.-W. Lee, J.-M. Han, M. Tanabe, T. Fujiwara, Y. Nakabayashi, G. Zhao, J. Zhang, K. Mima, X-ray astronomy in the laboratory with a miniature compact object produced by laser-driven implosion. *Nat. Phys.* **5**, 821–825 (2009).
5. B. A. Remington, D. Arnett, R. P. Drake, H. Takabe, Modeling astrophysical phenomena in the laboratory with intense lasers. *Science* **284**, 1488–1494 (1999).
6. A. B. Sefkow, G. R. Bennett, M. Geissel, M. Schollmeier, B. C. Franke, B. W. Atherton, Efficiency enhancement for K_α X-ray yields from laser-driven relativistic electrons in solids. *Phys. Rev. Lett.* **106**, 235002 (2011).
7. Y. Kitagawa, Y. Mori, O. Komeda, K. Ishii, R. Hanayama, K. Fujita, S. Okihara, T. Sekine, N. Satoh, T. Kurita, M. Takagi, T. Watari, T. Kawashima, H. Kan, Y. Nishimura, A. Sunahara, Y. Sentoku, N. Nakamura, T. Kondo, M. Fujine, H. Azuma, T. Motohiro, T. Hioki, M. Kakeno, E. Miura, Y. Arikawa, T. Nagai, Y. Abe, S. Ozaki, A. Noda, Direct heating of a laser-imploded core by ultraintense laser-driven ions. *Phys. Rev. Lett.* **114**, 195002 (2015).
8. R. Nora, W. Theobald, R. Betti, F. J. Marshall, D. T. Michel, W. Seka, B. Yaakobi, M. Lafon, C. Stoeckl, J. Delettrez, A. A. Solodov, A. Casner, C. Reverdin, X. Ribeyre, A. Vallet, J. Peebles, F. N. Beg, M. S. Wei, Gigabar spherical shock generation on the OMEGA laser. *Phys. Rev. Lett.* **114**, 045001 (2015).
9. T. R. Dittrich, O. A. Hurricane, D. A. Callahan, E. L. Dewald, T. Döppner, D. E. Hinkel, L. F. Berzak Hopkins, S. Le Pape, T. Ma, J. L. Milovich, J. C. Moreno, P. K. Patel, H.-S. Park, B. A. Remington, J. D. Salmonson, J. L. Kline, Design of a high-foot high-adiabat ICF capsule for the National Ignition Facility. *Phys. Rev. Lett.* **112**, 055002 (2014).

10. D. J. Hoarty, P. Allan, S. F. James, C. R. D. Brown, L. M. R. Hobbs, M. P. Hill, J. W. O. Harris, J. Morton, M. G. Brookes, R. Shepherd, J. Dunn, H. Chen, E. Von Marley, P. Beiersdorfer, H. K. Chung, R. W. Lee, G. Brown, J. Emig, Observations of the effect of ionization-potential depression in hot dense plasma. *Phys. Rev. Lett.* **110**, 265003 (2013).
11. P. M. Nilson, W. Theobald, J. F. Myatt, C. Stoeckl, M. Storm, J. D. Zuegel, R. Betti, D. D. Meyerhofer, T. C. Sangster, Bulk heating of solid-density plasmas during high-intensity-laser plasma interactions. *Phys. Rev. E Stat. Nonlinear Soft Matter Phys.* **79**, 016406 (2009).
12. D. J. Hoarty, S. F. James, C. R. D. Brown, B. M. Williams, H. K. Chung, J. W. O. Harris, L. Upcraft, B. J. B. Crowley, C. C. Smith, R. W. Lee, Measurements of emission spectra from hot, dense germanium plasma in short pulse laser experiments. *High Energy Density Phys.* **6**, 105–108 (2010).
13. C. R. D. Brown, D. J. Hoarty, S. F. James, D. Swatton, S. J. Hughes, J. W. Morton, T. M. Guymer, M. P. Hill, D. A. Chapman, J. E. Andrew, A. J. Comley, R. Shepherd, J. Dunn, H. Chen, M. Schneider, G. Brown, P. Beiersdorfer, J. Emig, Measurements of electron transport in foils irradiated with a picosecond time scale laser pulse. *Phys. Rev. Lett.* **106**, 185003 (2011).
14. V. Dervieux, B. Loupias, S. Baton, L. Lecherbourg, K. Glize, C. Rousseaux, C. Reverdin, L. Gremillet, C. Blancard, V. Silvert, J.-C. Pain, C. R. D. Brown, P. Allan, M. P. Hill, D. J. Hoarty, P. Renaudin, Characterization of near-LTE, high-temperature and high-density aluminum plasmas produced by ultra-high intensity lasers. *High Energy Density Phys.* **16**, 12–17 (2015).
15. K. U. Akli, S. B. Hansen, A. J. Kemp, R. R. Freeman, F. N. Beg, D. C. Clark, S. D. Chen, D. Hey, S. P. Hatchett, K. Highbarger, E. Giraldez, J. S. Green, G. Gregori, K. L. Lancaster, T. Ma, A. J. MacKinnon, P. Norreys, N. Patel, J. Pasley, C. Shearer, R. B. Stephens, C. Stoeckl, M. Storm, W. Theobald, L. D. Van Woerkom, R. Weber, M. H. Key, Laser heating of solid matter by light-pressure-driven shocks at ultrarelativistic intensities. *Phys. Rev. Lett.* **100**, 165002 (2008).
16. F. Y. Khattak, R. J. Clarke, E. J. Divall, M. Edwards, P. S. Foster, C. J. Hooker, A. J. Langley, P. Mistry, D. Neely, O. A. M. B. Percie du Sert, J. Smith, C. Spindloe, G. Tallents, M. Tolley, D. Riley, Enhanced He-α emission from "smoked" Ti targets irradiated with 400 nm, 45 fs laser pulses. *EPL* **72**, 242–248 (2005).
17. H. A. Sumeruk, S. Kneip, D. R. Symes, I. V. Churina, A. V. Belolipetski, T. D. Donnelly, T. Ditmire, Control of strong-laser-field coupling to electrons in solid targets with wavelength-scale spheres. *Phys. Rev. Lett.* **98**, 045001 (2007).
18. M. M. Murnane, H. C. Kapteyn, S. P. Gordon, J. Bokor, E. N. Glytsis, R. W. Falcone, Efficient coupling of high-intensity subpicosecond laser pulses into solids. *Appl. Phys. Lett.* **62**, 1068 (1993).
19. S. P. Gordon, T. Donnelly, A. Sullivan, H. Hamster, R. W. Falcone, X-rays from microstructured targets heated by femtosecond lasers. *Opt. Lett.* **19**, 484–486 (1994).
20. G. Kulcsár, D. AlMawlawi, F. W. Budnik, P. R. Herman, M. Moskovits, L. Zhao, R. S. Marjoribanks, Intense picosecond x-ray pulses from laser plasmas by use of nanostructured "velvet" targets. *Phys. Rev. Lett.* **84**, 5149–5152 (2000).
21. P. P. Rajeev, P. Taneja, P. Ayyub, A. S. Sandhu, G. R. Kumar, Metal nanoplasmas as bright sources of hard X-ray pulses. *Phys. Rev. Lett.* **90**, 115002 (2003).
22. S. Mondal, I. Chakraborty, S. Ahmad, D. Carvalho, P. Singh, A. D. Lad, V. Narayanan, P. Ayyub, G. R. Kumar, J. Zheng, Z. M. Sheng, Highly enhanced hard x-ray emission from oriented metal nanorod arrays excited by intense femtosecond laser pulses. *Phys. Rev. B* **83**, 035408 (2011).
23. T. Nishikawa, S. Suzuki, Y. Watanabe, O. Zhou, H. Nakano, Efficient water-window X-ray pulse generation from femtosecond-laser-produced plasma by using a carbon nanotube target. *Appl. Phys. B* **78**, 885–890 (2004).
24. M. A. Purvis, V. N. Shlyaptsev, R. Hollinger, C. Bargsten, A. Pukhov, A. Prieto, Y. Wang, B. M. Luther, L. Yin, S. Wang, J. J. Rocca, Relativistic plasma nanophotonics for ultrahigh energy density physics. *Nat. Photonics* **7**, 796–800 (2013).
25. A. P. Shevelko, X-ray spectroscopy of laser-produced plasmas using a von Hamos spectrograph. *Proc. SPIE* **3406**, 91–108 (1998).
26. D. Ryu, I. Chattopadhyay, E. Choi, Equation of state in numerical relativistic hydrodynamics. *Astrophys. J. Suppl. Ser.* **166**, 410–420 (2006).
27. V. Kaymak, A. Pukhov, V. N. Shlyaptsev, J. J. Rocca, Nanoscale ultradense Z-pinch formation from laser-irradiated nanowire arrays. *Phys. Rev. Lett.* **117**, 035004 (2016).
28. D. S. Clark, C. R. Weber, J. L. Milovich, J. D. Salmonson, A. L. Kritcher, S. W. Haan, B. A. Hammel, D. E. Hinkel, O. A. Hurricane, O. S. Jones, M. M. Marinak, P. K. Patel, H. F. Robey, S. M. Sepke, M. J. Edwards, Three-dimensional simulations of low foot and high foot implosion experiments on the National Ignition Facility. *Phys. Plasmas* **23**, 056302 (2016).
29. T. Ditmire, J. Zweiback, V. P. Yanovsky, T. E. Cowan, G. Hays, K. B. Wharton, Nuclear fusion from explosions of femtosecond laser-heated deuterium clusters. *Nature* **398**, 489–492 (1999).
30. J. P. Hoare, On the role of boric-acid in the Watts bath. *J. Electrochem. Soc.* **133**, 2491–2494 (1986).
31. A. Pukhov, Three-dimensional electromagnetic relativistic particle-in-cell code VLPL (Virtual Laser Plasma Lab). *J. Plasma Phys.* **61**, 425–433 (1999).
32. A. Zhidkov, A. Sasaki, Effect of field ionization on interaction of an intense subpicosecond laser pulse with foils. *Phys. Plasmas* **7**, 1341–1344 (2000).
33. A. Karmakar, A. Pukhov, Collimated attosecond GeV electron bunches from ionization of high-Z material by radially polarized ultra-relativistic laser pulses. *Laser Part. Beams* **25**, 371–377 (2007).
34. V. N. Shlyaptsev, J. J. G. Rocca, A. L. Osterheld, Dynamics of a capillary discharge x-ray laser. *Proc. SPIE* **2520**, 365–372 (1995).
35. M. Klapisch, M. Busquet, A. Bar-Shalom, A new and improved version of HULLAC. *AIP Conf. Proc.* **926**, 206 (2007).
36. L. M. Biberman, V. S. Vorob'ev, I. T Yakubov, *Kinetics of Nonequilibrium Low-Temperature Plasmas* (Springer, 1987), 498 pp.
37. T. Holstein, Imprisonment of resonance radiation in gases. *Phys. Rev.* **72**, 1212–1233 (1947).
38. J. L. Synge, *The Relativistic Gas* (North-Holland Publishing Co., 1957).

Acknowledgments: We acknowledge M. Purvis for helpful discussions. **Funding:** This work was funded by the High Energy Density Laboratory Plasmas program, Fusion Energy Sciences, Office of Science of the U.S. Department of Energy (grant DE-SC0014610), and a previous grant from the Defense Threat Reduction Agency (grant HDTRA-1-10-1-0079). The work of Lawrence Livermore National Laboratory researchers was performed under the auspices of the U.S. Department of Energy under contract no. DE-AC52-07NA27344. **Author contributions:** The concept of the experiment was proposed by J.J.R., and the experiment was designed by J.J.R., C.B., and R.H. Modeling was performed by V.N.S., V.K., A.P., and R.L. using atomic data computed by M.B. and M.K. The targets were developed and manufactured by C.B., M.G.C., and D.K. The experiments and related measurements were conducted by C.B., R.H., S.W., A.R., Y.W., R.T., J.P., and J.J.R. All authors participated in the writing of the manuscript. **Competing interests:** The authors declare that they have no competing interests. **Data and materials availability:** All data needed to evaluate the conclusions in the paper are present in the paper and/or the Supplementary Materials. Additional data related to this paper may be requested from the authors.

Submitted 7 July 2016
Accepted 28 November 2016
Published 11 January 2017
10.1126/sciadv.1601558

Citation: C. Bargsten, R. Hollinger, M. G. Capeluto, V. Kaymak, A. Pukhov, S. Wang, A. Rockwood, Y. Wang, D. Keiss, R. Tommasini, R. London, J. Park, M. Busquet, M. Klapisch, V. N. Shlyaptsev, J. J. Rocca, Energy penetration into arrays of aligned nanowires irradiated with relativistic intensities: Scaling to terabar pressures. *Sci. Adv.* **3**, e1601558 (2017).

ScienceAdvances
AAAS

Energy penetration into arrays of aligned nanowires irradiated with relativistic intensities: Scaling to terabar pressures

Clayton Bargsten, Reed Hollinger, Maria Gabriela Capeluto, Vural Kaymak, Alexander Pukhov, Shoujun Wang, Alex Rockwood, Yong Wang, David Keiss, Riccardo Tommasini, Richard London, Jaebum Park, Michel Busquet, Marcel Klapisch, Vyacheslav N. Shlyaptsev and Jorge J. Rocca (January 11, 2017)

Sci Adv 2017, 3:.
doi: 10.1126/sciadv.1601558